Journal Pre-proof

YWHAE loss of function causes a rare neurodevelopmental disease with brain abnormalities in human and mouse

Anne-Sophie Denommé-Pichon, Stephan C. Collins, Ange-Line Bruel, Anna Mikhaleva, Christel Wagner, Valerie E. Vancollie, Quentin Thomas, Martin Chevarin, Mathys Weber, Carlos E. Prada, Alexis Overs, María Palomares-Bralo, Fernando Santos-Simarro, Marta Pacio-Míguez, Tiffany Busa, Eric Legius, Carlos A. Bacino, Jill A. Rosenfeld, Gwenaël Le Guyader, Matthieu Egloff, Xavier Le Guillou, Maria Antonietta Mencarelli, Alessandra Renieri, Salvatore Grosso, Jonathan Levy, Blandine Dozières, Isabelle Desguerre, Antonio Vitobello, Yannis Duffourd, Christopher J. Lelliott, Christel Thauvin-Robinet, Christophe Philippe, Laurence Faivre, Binnaz Yalcin

PII: S1098-3600(23)00848-1

DOI: https://doi.org/10.1016/j.gim.2023.100835

Reference: GIM 100835

To appear in: *Genetics in Medicine*

Received Date: 10 October 2022

Revised Date: 20 March 2023

Accepted Date: 23 March 2023

Please cite this article as: Denommé-Pichon AS, Collins SC, Bruel AL, Mikhaleva A, Wagner C, Vancollie VE, Thomas Q, Chevarin M, Weber M, Prada CE, Overs A, Palomares-Bralo M, Santos-Simarro F, Pacio-Míguez M, Busa T, Legius E, Bacino CA, Rosenfeld JA, Le Guyader G, Egloff M, Le Guillou X, Mencarelli MA, Renieri A, Grosso S, Levy J, Dozières B, Desguerre I, Vitobello A, Duffourd Y, Lelliott CJ, Thauvin-Robinet C, Philippe C, Faivre L, Yalcin B, YWHAE loss of function causes a rare neurodevelopmental disease with brain abnormalities in human and mouse, *Genetics in Medicine* (2023), doi: https://doi.org/10.1016/j.gim.2023.100835.

YWHAE loss of function causes a rare neurodevelopmental disease with brain abnormalities in human and mouse

Anne-Sophie Denommé-Pichon[1,2,3*], Stephan C. Collins[2*], Ange-Line Bruel[1,2*], Anna Mikhaleva[4], Christel Wagner[5], Valerie E. Vancollie[6], Quentin Thomas[2,7,8], Martin Chevarin[1,2], Mathys Weber[2,7], Carlos E. Prada[9], Alexis Overs[1,2], María Palomares-Bralo[3,10,11], Fernando Santos-Simarro[3,10,11], Marta Pacio-Míguez[11], Tiffany Busa[12], Eric Legius[13], Carlos A. Bacino[14], Jill A. Rosenfeld[14,15], Gwenaël Le Guyader[16], Matthieu Egloff[16,17], Xavier Le Guillou[16], Maria Antonietta Mencarelli[18], Alessandra Renieri[18,19,20], Salvatore Grosso[21,22], Jonathan Levy[23], Blandine Dozières[24], Isabelle Desguerre[25], Antonio Vitobello[1,2,3], Yannis Duffourd[1,2], Christopher J. Lelliott[6], Christel Thauvin-Robinet[1,2,26], Christophe Philippe[1,2], Laurence Faivre[2,3,7‡], Binnaz Yalcin[2‡]

1 Unité Fonctionnelle Innovation en Diagnostic génomique des maladies rares, FHU-TRANSLAD, CHU Dijon Bourgogne, Dijon, France
2 UMR1231 GAD, Inserm - Université Bourgogne-Franche Comté, Dijon, France
3 European Reference Network, ERN ITHACA
4 Center for Integrative Genomics, University of Lausanne, CH-1015 Lausanne, Switzerland
5 IGBMC, UMR7104, Inserm, U964, 67400 Illkirch, France
6 Wellcome Sanger Institute, Hinxton, Cambridge, CB10 1SA, United Kingdom
7 Centre de Référence Maladies Rares « Anomalies du développement et syndromes malformatifs », Centre de Génétique, FHU-TRANSLAD et Institut GIMI, CHU Dijon Bourgogne, Dijon, France
8 Department of Neurology, Dijon Bourgogne University Hospital, F-21000 Dijon, France
9 Division of Genetics, Birth Defects & Metabolism, Ann & Robert H. Lurie Children's Hospital of Chicago, Chicago, Illinois, USA
10 Instituto de Genética Médica y Molecular (INGEMM), Hospital Universitario La Paz, Universidad Autónoma de Madrid, IdiPAZ, Madrid, Spain
11 Centro de Investigación Biomédica en Red de Enfermedades Raras (CIBERER, U753), Instituto Carlos III, Madrid, Spain
12 Département de génétique médicale, CHU Timone enfants, AP-HM, Marseille, France
13 Laboratory for Neurofibromatosis Research, Department of Human Genetics, KU Leuven University Hospital, Belgium
14 Department of Molecular and Human Genetics, Baylor College of Medicine, Houston, TX 77030, USA
15 Baylor Genetics Laboratories, Houston, TX, USA
16 CHU Poitiers, Service de Génétique, BP577, 86021 Poitiers, France; Université Poitiers, 86034 Poitiers, France
17 Laboratoire de Neurosciences Experimentales et Cliniques, INSERM, Poitiers, France.
18 Genetica Medica, Azienda Ospedaliera Universitaria Senese, Siena, Italy
19 Medical Genetics, University of Siena, Siena, Italy
20 Med Biotech Hub and Competence Center, Department of Medical Biotechnologies, University of Siena, Siena, Italy
21 Dipartimento di Medicina Molecolare e dello Sviluppo, Universita' degli Studi di Siena, viale Bracci 16, 53100, Siena, Italy

22 U.O.C. Pediatria, Azienda Ospedaliera Universitaria Senese, viale Bracci 16, 53100, Siena, Italy
23 Genetics Department, APHP, Robert-Debré University Hospital, Paris, France.
24 AP-HP, Hôpital Robert Debré, Service de Neurologie Pédiatrique et des Maladies Métaboliques, 75019 Paris, France.
25 Departments of pediatric neurology and medical genetics, Hospital Necker-Enfants Malades, Université Paris Cité, F-75015, Paris France
26 Centre de Référence Déficiences Intellectuelles de Causes Rares, FHU-TRANSLAD, CHU Dijon Bourgogne, France

* these authors contributed equally to this work
‡ these authors have equally co-directed this work

Corresponding authors

Dr Anne-Sophie Denommé-Pichon, MD
Unité Fonctionnelle Innovation en Diagnostic génomique des maladies rares, FHU-TRANSLAD, CHU Dijon Bourgogne, 15 boulevard Maréchal De Lattre de Tassigny, 21070 Dijon CEDEX, France
Phone: +33 3 80 39 32 38 / Fax: +33 3 80 29 32 66
E-mail: anne-sophie.denomme-pichon@u-bourgogne.fr

Dr Binnaz Yalcin, PhD
INSERM UMR 1231, University of Burgundy, 21000, Dijon, France
Phone : +33 3 80 39 66 60
E-mail: binnaz.yalcin@inserm.fr

Keywords

Neurodevelopmental disorders, Miller-Dieker syndrome, brain abnormalities, knockout mouse model, YWHAE, 14-3-3

Abstract

Purpose

Miller-Dieker syndrome is caused by a multiple-gene deletion, including *PAFAH1B1* and *YWHAE*. While deletion of *PAFAH1B1* causes lissencephaly unambiguously, deletion of *YWHAE* alone has not clearly been linked to a human disorder.

Methods

Cases with *YWHAE* variants were collected through international data-sharing networks. To address the specific impact of *YWHAE* loss of function, we phenotyped a mouse knockout of *Ywhae*.

Results

We report a series of 10 individuals with heterozygous loss-of-function *YWHAE* variants (3 SNVs, 7 deletions <1 Mb encompassing *YWHAE* but not *PAFAH1B1*), including 8 new cases and 2 follow-ups, added with 5 cases (CNVs) from literature review. While, until now, only one intragenic deletion has been described in *YWHAE*, we report 4 new variants specifically in *YWHAE* (3 splice variants and 1 intragenic deletion). The most frequent manifestations are developmental delay, delayed speech, seizures and brain malformations including corpus callosum hypoplasia, delayed myelination, ventricular dilatation. Individuals with variants affecting *YWHAE* alone have milder features than those with larger deletions.

Neuroanatomical studies in *Ywhae*$^{-/-}$ mice revealed brain structural defects including thin cerebral cortex, corpus callosum dysgenesis, hydrocephalus paralleling those seen in humans.

Conclusion

This study further demonstrates that *YWHAE* loss-of-function variants cause a neurodevelopmental disease with brain abnormalities.

Introduction

Miller-Dieker syndrome (MDS; [MIM #247200]) is a contiguous gene deletion syndrome due to a microdeletion involving 26 coding genes on human chromosome 17p13.3, including both *PAFAH1B1* and *YWHAE* (1–3). MDS is characterized by neurodevelopmental delay with classical lissencephaly type 1, microcephaly, brain abnormalities, seizures, and craniofacial abnormalities including a narrow and furrowing forehead, low-set and posteriorly rotated ears, small eyes, upslanting palpebral fissures, epicanthus, a small nose with low nasal bridge, upturned nares, thin upper lip, cleft palate and small chin. Additional manifestations include cardiac malformations, urogenital abnormalities and a failure to thrive. Lifespan is drastically shortened, with few patients surviving past early childhood (4).

Smaller deletions or loss-of-function variants involving the proximal *PAFAH1B1* gene alone (formerly named *LIS1* [MIM *601545]) are responsible for isolated lissencephaly (LIS1; [MIM #607432]) (5), making *PAFAH1B1* the main determinant for lissencephaly in patients with MDS. While the *PAFAH1B1*-associated clinical features are well documented, the specific contribution of the *YWHAE* gene to MDS is understudied. Apart from one single-case report with a small 12.6 kb intragenic deletion of the *YWHAE* gene presenting brain abnormalities (6), the link between *YWHAE* variants alone and human disorders remains understudied, showing a need to build a cohort of individuals with *YWHAE* variants alone.

The *YWHAE* gene (tyrosine 3-monooxygenase/tryptophan 5-monooxygenase activation protein, epsilon isoform [MIM *605066]) encodes the 14-3-3 epsilon protein. 14-3-3ε is highly conserved and implicated in intracellular events involving phosphorylation-dependent switching or protein-protein interactions (7). 14-3-3ε is widely expressed throughout the body and at very high levels in various cell types of the central nervous system (8) where 14-3-3 proteins were originally discovered.14-3-3ε interacts with doublecortin (9), NUDEL, LIS1 and

dynein (10). Its overexpression result in defects in neurite formation (9). In human, duplications involving *YWHAE* and the adjacent genes have been associated to an increased risk of mild developmental delay (11). *In vivo*, 14-3-3ε is associated with increased motor activity and decreased working memory in mice (12,13). 14-3-3ε is involved in corticogenesis and neuronal migration in the CA3 layer of the hippocampus by binding to the NUDEL protein (10). 14-3-3ε regulates neurogenesis and differentiation of neuronal progenitor cells in the developing mouse brain (14). The auditory brainstem response shows that mouse *Ywhae* is also involved in hearing and mutant mice have increased minimum detection thresholds at all frequencies (15).

Here we report and analyze a series of 10 patients, along with 5 cases previously published, with heterozygous loss-of-function *YWHAE* variants collected through international collaborations. The effect of the *YWHAE* loss of function is further investigated through phenotypic characterization of a homozygous knockout mouse model we generated at the Wellcome Sanger Institute (UK). Together, our results establish a new neurodevelopmental disease caused by loss-of-function *YWHAE* variants both in human and mouse.

Materials and methods

Human

Patient recruitment

Written informed consent for study participation and publication was obtained by the attending geneticist or the referring physician from the patients' legal guardians.

Collection of cases: data sharing networks

Cases were collected through data sharing networks. The cases included in this study were gathered through GeneMatcher (16), the Decipher database, the ITHACA European Reference Network, the French AnDDI-Rares network and through personal correspondence. We included cases with single nucleotide variants (SNVs) in *YWHAE* or deletions of less than 1 Mb encompassing *YWHAE* but not *PAFAH1B1*. We chose not to include cases with *PAFAH1B1* deletion to increase detection power of phenotypes specific to *YWHAE*.

Clinical characteristics were assessed through a standardized phenotyping sheet and included data on MRI neuroimaging.

Genetic testing and targeted RNA study

In all patients, variants and deletions disrupting *YWHAE* were detected by either chromosomal microarray analysis (CMA) or next generation sequencing (NGS). For a description of CMA and NGS methodology, see the supplemental methods. All variants reported in this study refer to *YWHAE* transcript NM_006761.5. Genomic coordinates refer to the GRCh37 human reference genome. SNVs were classified using American College of Medical Genetics and Genomics (ACMG) guidelines (17).

For the cases with SNVs, we set out to assess the variant's impact on splicing. Cases 2 and 3 (two monozygotic twins carrying the same variant) underwent targeted RNA study. Total RNA was extracted from whole blood collected in a PAXgene tube (Preanalytics GmbH, Hombrechtikon, Switzerland) using the PAXgene Blood RNA kit (Preanalytics GmbH, Hombrechtikon, Switzerland) following the standard protocol. cDNA was obtained using the QuantiTect Reverse Transcription kit (Qiagen GmbH, Hilden, Germany). RNA from case 1 was not available and has not been studied. The conditions for reverse transcription PCR (RT-PCR) are detailed in the supplemental methods.

Phenotypic features comparison

Patients for whom a specific feature information was missing were not included in that feature's statistic, hence the group sizes differ between features. We used the Fenton preterm growth charts with term-corrected age to assess birth measurements and WHO growth charts from 0 to 5 years and from 1 to 18 years to assess measurements after birth.

Mouse

Generation of *Ywhae* knockout mouse model

The knockout mouse model was generated by homologous recombination using the knockout-first allele method, producing the *Ywhae*$^{\text{tm1e(EUCOMM)Wtsi}}$ knockout allele. The *Ywhae* gene was targeted in C57BL/6N embryonic stem cells with a conditional-ready cassette (clone EPD0200_5_G01) as described previously (18). Germ line transmission was confirmed by a series of genotyping and quantitative PCR analyses using the standard IMPC (International Mouse Phenotyping Consortium) QC validation strategy, with the results found here (https://www.mousephenotype.org/data/genes/MGI:894689). Mice derived from heterozygous (Het) intercross were genotyped for the *Ywhae*^{tm1e} allele by PCR carried out as previously described (19). On a C57BL/6N background, Het mice were sub-viable: 20 Het mice out of 192 offspring were obtained from Het x Wildtype (WT) matings at weaning (15). The line was then crossed with 129S5/SvEvBrd/Wtsi in order to improve viability. Mice were produced from Het x Het matings to give segregating litters that included homozygous knockout (Hom), Het and WT as littermate controls. A subset of these mice was used in neuroanatomical characterization.

Mouse whole-body phenotyping studies

The *Ywhae*$^{\text{tm1e(EUCOMM)Wtsi}}$ knockout mice were phenotyped for whole-body traits by the Mouse Genetics Project (MGP) pipeline at the Wellcome Sanger Institute, UK (for details, see the supplemental methods). In brief, mice of both sexes were weighed between 4 and 16 weeks of age and assessed at 9 weeks for gross behavioral abnormalities (modified SHIRPA (20)) and

dysmorphology using standardized procedures. For each test, *Ywhae*$^{tm1e/tm1e}$ were tested alongside littermate *Ywhae*$^{+/+}$ controls through the pipeline which included tests for indirect calorimetry, body composition, X-ray morphology, blood chemistry and hematology (n=6 for WT and n=7 for Hom mice).

Comprehensive neuroanatomical studies

Neuroanatomical studies were carried out using 3 male *Ywhae*$^{tm1e/tm1e}$ and 5 WT male mice (2 littermates and 3 mice from the same mixed background) at 16 weeks of age. Mice were anesthetized with ketamine (100 mg/kg, intraperitoneal) and xylazine (10 mg/kg, intraperitoneal). Brains were dissected and fixed in 4% neutral buffered formalin for 48 hours, then transferred to 70% ethanol. Samples were embedded in paraffin using an automated embedding machine (Sakura Tissue-Tek VIP) and cut at a thickness of 5 µm with a sliding microtome (Leica RM 2145) in order to obtain coronal brain region at Bregma +0.98 mm according to the Allen Mouse Brain Atlas (21). The sections were then stained with 0.1% Luxol Fast Blue (Solvent Blue 38; Sigma-Aldrich) and 0.1% cresyl violet acetate (Sigma-Aldrich), and scanned using Nanozoomer 2.0HT, C9600 series at 20X resolution, as previously described (22).

Image analysis

Twenty-two brain parameters, made up of area and length measurements, were taken blind to the genotype. Using in-house ImageJ plugins, an image analysis pipeline was used to standardize measurements. Each image was quality controlled for the accuracy of sectioning relative to the reference Allen Mouse Brain Atlas and controlled for asymmetries and histological artifacts (23). At Bregma +0.98 mm, brain structures assessed were: 1) the total brain area, 2) the lateral ventricles, 3) the cingulate cortex, 4) the genu of the corpus callosum, 5) the caudate putamen, 6) the anterior commissure, 7) the piriform cortex, 8) the primary motor cortex and 9) the secondary somatosensory cortex. All samples were also systematically

assessed for cellular ectopia (misplaced neurons). Mouse neuroanatomical data was analyzed using a two-tailed Student's t-test assuming equal variance.

Mouse embryogenesis and High-Resolution Episcopic Microscopy (HREM)

To study mouse embryogenesis, we generated Het x Het timed matings on a mixed C57BL/6N and 129S5/SvEvBrd/Wtsi genetic background. We produced 44 embryos at embryonic day 14.5 (E14.5), of which 3 Hom and 3 WT were sent to the Deciphering the Mechanisms of Developmental Disorders consortium (DMDD, https:/dmdd.org.uk) for HREM processing. The detailed protocol has been published previously (24). Briefly, 14.5-day embryos were embedded in a hard plastic resin, enabling thin sectioning (1 µm). This resin contains a fluorescent dye allowing contrast between the tissue and the bright background of the plastic. By sequentially imaging the block face during the sectioning process, a comprehensive stack of accurately aligned images was acquired, documenting the 3D structure of the sample. We then carried out a comprehensive assessment of brain morphometrics adapting our 2D histology protocol used in adult mice to 3D brain stacks (25).

Results

We present a series of 8 new and 2 follow-ups, along with 5 other previously published cases from a literature review (6,26–31). In total, 15 patients (7 males, 7 females, 1 unknown) from 14 unrelated families with heterozygous loss-of-function *YWHAE* variants were collected: 3 splice site variants (cases 1 to 3), 2 intragenic deletions (cases 10 and 14) and 10 large deletions (<1 Mb) encompassing *YWHAE* but not *PAHAFAB1* (cases 4 to 9, 11 to 13 and 15) (**Figure 1A** and **1B**).

Variants occurred *de novo* (10/12) or were inherited from a symptomatic parent (1/12) or from a healthy father with paternal mosaicism (1/12). In 3/15 cases, inheritance is not known.

The c.715+1G>T variant present in cases 2 and 3 affects the donor splice site of intron 5 of *YWHAE*. Analysis of RT-PCR products from cases 2 and 3 by gel electrophoresis showed two bands corresponding to two RNAs of different sizes (**Figure 1C**). The study of variant impact on pre-messenger RNA splicing using targeted cDNA sequencing showed the skipping of exon 5 (NM_006761.4:r.579_715del) in a heterozygous state, with 40920/87290 reads in case 2 and 10437/22352 reads in case 3, leading to the deletion of 127 nucleotides, predicted to cause a frameshift and create a premature stop codon p.(Leu194*) (**Figure 1C**). These additional results confirm that the c.715+1G>T variant results in an aberrant splicing of the *YWHAE* gene.

The main clinical features are summarized in **Table 1** and fully detailed in **Table 2**. The mean age at the time of the last evaluation was 10 years (from 19 weeks of gestation to 39 years old). There was no apparent difference in severity between males and females. Almost all patients had developmental delay (13/14) with impaired speech or language (11/11). The age of the first sentences ranged from 2 years 6 months to 3 years 4 months (mean of 2 years 7 months). Motor delay was less common: 3/10 started to walk after 18 months (from before 12 to 30 months), 3/8 had impaired gait and 4/7 impaired hand skills like dyspraxia (2/7). When present and evaluable, intellectual disability (ID) (6/13) was mild to severe and, interestingly, variants strictly within *YWHAE* were associated with ID in only one case (case 1), presenting with mild ID. Behavioral disorders were frequent (6/12) and some patients were reported with ADHD (3/12) and anxiety (3/12). Growth retardation was observed only in patients with a deletion encompassing more than just *YWHAE* (4/11). Hypotonia seemed to be frequent (7/12), accompanied by feeding difficulties in two patients. Tremor was reported (2/11). Seizures were frequent (8/13) with a mean age of onset of 2.4 years (from 4.5 months to 9 years). Seizures were tonico-clonic, myoclonic, spams, absence or febrile. Some individuals had several types of seizure and 2/8 patients presented with multi-daily seizures. Brain malformations were common (8/12) (**Figure 2A**) and included signs of altered myelination (ventricular dilation

(3/8), corpus callosum hypoplasia (5/8), poor myelination (3/8)), cysts (subependymal germinolytic, septum pellucidum, cavum vergae, arachnoid, near optic nerve) (4/8), cerebellar hypoplasia (3/8), enlarged Virchow-Robin spaces (3/8), thinning of the frontal cortex (2/8), absence of the olfactory bulbs (2/8), Chiari malformation type 1 (1/8), intraventricular hemorrhage (1/8), pituitary hypoplasia (1/8), polymicrogyria (1/8) and nodular heterotopias (1/8). Craniofacial features were observed in 12/15 patients, among which 3/5 with variants strictly within *YWHAE*, presenting milder and non-specific dysmorphic features (**Figure 2B**). Skeletal defects were observed in 7/13 patients, with clinodactyly or camptodactyly of the 4th or the 5th fingers in 4/7 individuals. While individuals did not have their hearing tested, no impairments were reported.

We next thought to characterize and evaluate datasets from a *Ywhae*$^{\text{tm1e(EUCOMM)Wtsi}}$ knockout mouse model with a focus on the most frequent clinical components of the human disorder. Results of knockout mice from this study and a literature review are summarized in **Table 1** (9,12,13,10,14,15). According to the literature, phenotypes were more severe in *Ywhae*$^{-/-}$ mutants when compared to *Ywhae*$^{+/-}$ mice. With respect to the 3Rs (replacement, reduction and refinement) principles to limit animal use, heterozygous *Ywhae*^{tm1e} mutant mice were not studied as our main goal was to gain insights into the *in vivo* consequences of *YWHAE* full inactivation. In our previous research, *Ywhae*$^{tm1e/tm1e}$ mice showed reduced body weight from weaning age at all time points until 16 weeks of age (**Figure 3A** adapted from (15)). The area under the curve was 22% lower in *Ywhae*$^{tm1e/tm1e}$ compared to WT animals ($p<0.05$, t-test). At 12 weeks, these differences were mostly driven by a reduction in body length and lean body mass (-8%, $p<5.10^{-5}$ and -15%, $p<5.10^{-3}$, respectively) (**Figure 3B-C**). To determine if these growth delays might also occur during embryogenesis, we assessed embryo morphology in a group of 13 homozygous embryos out of the 44 collected. We found 23% (3/13) exhibited

embryonic growth retardation, 38.5% (5/13) presented with a fetal edema and 31% (4/13) displayed a pale yolk sack (data not shown), suggesting that growth delays originate from embryonic stages.

Food consumption was measured over 21 hours in metabolic cages and *Ywhae*$^{tm1e/tm1e}$ mice displayed a reduced latency to feeding initiation (**Figure 3D**). Water intake however was normal (data not shown). After 5 hours, the cumulative food intake resumed with similar increments compared to WT, highlighting that the earlier increase in food intake could be the result of hyperactivity which has been reported before (12,13). Thus, the trend towards increase in food consumption does not mirror fat mass (**Figure 3E**) or fat percentage (24.4% ±2.5 *versus* 21% ±3.2 in WT and *Ywhae*$^{tm1e/tm1e}$, respectively) which were identical in both genotypes. Instead, body length and lean mass were significantly reduced (-8%, $p<10^{-4}$ and -16%, $p<0.005$, respectively), highlighting growth delay. Indirect calorimetric analysis in individual cages highlighted hyperactivity at night (**Supplementary Figure** and **Supplementary Table 1**). The respiratory exchange ratio (RER) was slightly elevated in *Ywhae*$^{tm1e/tm1e}$ mice, indicative of greater use of carbohydrates as a substrate, and could again be correlated to hyperactivity since this feature was only present for low RER readings and only during the first 5 hours of the acclimatization period (**Supplementary Figure**). This suggests that physical alterations in *Ywhae*$^{tm1e/tm1e}$ mice result from developmental abnormalities rather than a metabolic origin. Standard measures of plasma metabolites showed an increase in sodium (+2%), glycerol (+48%), alkaline phosphatase (+41%) and aspartate aminotransferase (+42%) (**Supplementary Table 2**). Hematology profiles showed increased white and red blood cell counts (+48% and +12%, respectively) (**Supplementary Table 3**). Bone area and mineral content showed a reduction (-19.2%, $p<10^{-6}$ and -22.9%, $p<10^{-4}$, respectively), whilst bone density was not affected (not significant) (**Figure 3F-H**). Except for a shortened skull and a concave nasal spline, the bone shape and morphology assessed by radiography (**Supplementary Table 4**) and

other variables such as coat and skin color, head size and morphology, fore- and hindlimb size and morphology, digit fusion and nail counts were normal in *Ywhae*$^{tm1e/tm1e}$ mice.

A previous study reported an abnormal morphology of the hippocampus when *Ywhae* is inactivated in the mouse (10). In the present study, comprehensive neuroanatomical phenotyping of adult and embryos *Ywhae*$^{tm1e/tm1e}$ mice allowed us to find new features relevant to human *YWHAE* variants that have not been reported before.

Among the 22 brain parameters assessed at Bregma +0.98 mm, severe and multiple brain defects including microcephaly were identified in male *Ywhae*$^{tm1e/tm1e}$ mice and are summarized in **Figure 3I-J**. The total brain area at Bregma +0.98 mm was reduced (-18%, p=0.02). Strikingly, mutant mice showed a compression of the genu of the corpus callosum width (-67%, $p=10^{-5}$) associated with enlarged lateral ventricles (+394% on average, $p<10^{-4}$) (**Figure 3K**). In addition, we observed an unusual mass of axons ventrally contiguous to the midline of the corpus callosum (black arrow, **Figure 3K**) that could potentially originate from dysregulation in the navigation of post-crossing axons in the corpus callosum as previously described (32). Fronto-medio-dorsal cortical areas were also reduced in size with the cingulate cortex area, width and height all being significantly affected ($p<0.05$). Interestingly, white matter structures were also reduced in size independently of local pressure from other parameters. This was the case for the anterior commissure (-43%, $p<10^{-4}$) which is situated on the floor of the caudate putamen (not significant). Basic neurological assessment did not reveal any gross abnormalities (**Supplementary Table 5**) although not every neurological function was tested since it has been extensively published elsewhere (13). To discriminate congenital brain malformations from acquired brain abnormalities (when the brain is normal at birth but shows abnormalities subsequently), we studied brain morphology at embryonic day 14.5 (E14.5) using High-Resolution Episcopic Microscopy (HREM) datasets (**Figure 3L**). More specifically, we reassessed phenotypes present in adults using the murine developmental brain atlas (33) and

online software available through the DMDD website. Lateral ventricle enlargement was clearly visible on parasagittal planes whilst thinning of cortical layers (cortical plate and cortical subventricular layer) was also evident on coronal sections (black arrows, **Figure 3L**). Together, these results indicate that neuroanatomical defects pertaining to ventricles, white matter structures and brain size originate early during embryonic life.

Discussion

Here we report clinical manifestations of 15 patients with clear dose-dependent loss-of-function variants in *YWHAE*, 5 of which are patients with variants affecting only *YWHAE* showing developmental and speech delays (5/5), as well as brain malformations (4/4), establishing *YWHAE* as a gene causing a rare neurodevelopmental disease. 3/15 of the patients carried splice variants, while 12/15 had deletions encompassing the *YWHAE* gene (2 small intragenic and 10 larger deletions encompassing additional genes in 17p13.3). When the inheritance was known, variants occurred *de novo* with the exception of two variants inherited from a symptomatic parent or a healthy mosaic father.

We did not identify any recurrent variant – except for the one present in the two monozygotic twins – nor did we identify pathogenic nonsense, missense or indel variants in *YWHAE*. Some regions of *YWHAE* present a strong constraint to missense variants since they do not seem to tolerate any such variant (gnomAD v2.1.1) (34). Although we only identified loss-of-function variants in *YWHAE*, we do not exclude the possibility that missense variants could also alter 14-3-3ε protein function. It is noteworthy that the Decipher (ID 359873, 288974) and ClinVar (VCV000148756, VCV000154956) databases show 4 additional deletions of *YWHAE* alone, one of which (VCV000154956) is located in coding regions, reported in an individual with autistic behavior. No further clinical details and inheritance information are provided on these

online databases although autism is known to be associated with disorders of the corpus callosum (35).

We are aware of only one case reported in the literature with a deletion of *YWHAE* alone (6). We identified 4 additional individuals with *YWHAE* variants alone bringing the total number of patients with specific variants in *YWHAE* to 5. This allowed a better delineation of the core phenotypes associated specifically with *YWHAE* loss of function which consistently included global developmental delay with impaired language, hypotonia and brain malformations including corpus callosum hypoplasia, delayed myelination and ventricular dilatation (see **Table 1** for a summary or **Table 2** for a detailed phenotypic description). We found notable neuroanatomical phenotypic overlap with homozygous *Ywhae*$^{tm1e/tm1e}$ mutant mice which displayed multiple brain structure defects including hydrocephaly, dysgenesis of the corpus callosum, small anterior commissure and thin motor and cingulate cortices, present before birth. The novelty of our murine findings in the context of previous *Ywhae* mouse reports (9,10,12–15) lies in the comprehensive assessment of neuroanatomical phenotypes relying on a newly developed precision histology approach (25), allowing us to detect more subtle neuroanatomical differences (see **Figure 3K** for an example).

Seizures and behavioral abnormalities were commonly present in patients (see **Table 1**). Dysmorphic facial features seem to be milder when compared to individuals with deletion encompassing more than just *YWHAE*. Only one patient out of five presented with mild intellectual disability. Cases with a variant specifically in *YWHAE* did not show growth retardation in contrast to patients with more than one gene affected that included the *CRK* gene previously reported to be associated with growth retardation in the Miller-Dieker syndrome (30). Intriguingly, *Ywhae*$^{tm1e/tm1e}$ mice exhibited a reduced body weight in line with previous knockout mouse studies on different genetic backgrounds (10,13,15). No gross behavioral abnormalities using the modified SHIRPA procedure (20) were seen in our mice and epilepsy

was not modeled. However, in a previous study dedicated to neurocognitive behaviors in *Ywhae* homozygous knockouts, mice showed increased locomotor activity and deficits in cognition (13).

Although the precise molecular role of 14-3-3ε in the development of the corpus callosum remains unclear, it has been shown that 14-3-3 proteins regulate the switch from sonic hedgehog-mediated commissural axon attraction to repulsion after midline crossing in the developing mouse spinal cord (36). The involvement of 14-3-3ε in a switch that controls repulsive guidance clues was further evidenced in motor axons derived from the fruit fly CNS model system (37). It is thus tempting to speculate that the mass of axons we detected beneath the corpus callosum (black arrow, **Figure 3K**) may be due to mis-regulation of commissural axon attraction and repulsion, potentially caused by the absence of 14-3-3ε. Through its interactions with LIS1 and NUDEL, 14-3-3ε is also known to interact with dynein. When 14-3-3ε is deficient in mice, there is a reduction in cytoplasmic dynein function, thereby underlining its role in neuronal migration (10,38). Via its interactions with dynein, it could be hypothesized that loss of 14-3-3ε could affect corticogenesis and explain the thinning of the motor and cingulate cortices in mice. However, further analyses should be performed to study the precise function of 14-3-3ε protein in corticogenesis and colossal axon crossing at the midline.

Conclusion

This study presents the first molecular and clinical description of a rare neurodevelopmental disorder occurring with brain abnormalities caused by heterozygous loss-of-function SNVs in *YWHAE*, and gathers new or previously reported cases with deletion encompassing *YWHAE* but not *PAFAH1B1*. Moreover, studies of *Ywhae*$^{tm1e/tm1e}$ mice showed neuroanatomical defects

similar to those seen in the human condition, reinforcing the importance of *YWHAE* in the proper development of the mammalian brain.

Together, these results suggest that *YWHAE* loss of function results in a neurodevelopmental syndrome with brain abnormalities involving corpus callosum dysgenesis with milder phenotypes than the contiguous gene deletion syndrome of chromosome 17p13.3 without the *PAFAH1B1* deletion.

To improve the identification and management of this new syndrome, the clinical data would need to be enriched, in particular with respect to the neurocognitive profile and the long-term outcome of these patients.

Legends

Table 1. Comparative summary of clinical features between individuals with variants in *YWHAE* only, individuals with variants in *YWHAE* and other genes, and Ywhae$^{tm1e/tm1e}$ mice, from this study and a literature review (9,10,12–15). The severity of the signs increases with the number of "+" symbols. The symbol +/- indicates inconsistent results between mouse studies which we briefly comment on here: for the assessment of anxiety, Ikeda *et al.* (12) used the elevated plus maze whereas Wachi *et al.* (13) the open field test; for growth retardation, the effect of the Ikeda *et al.*'s study was mild (12), so it could be a false positive. To facilitate the interpretation of the murine findings, we also provide the full nomenclature of the models used in the literature review: for Toyo-Oka *et al*. 2003, allele designation *Ywhae*^{tm1Awb}, genetic background 129S6/SvEvTac × NIH Black Swiss (10); for Ikeda *et al*. (12) same as Toyo-Oka *et al*. 2003; for Cornell *et al*. and Toyo-Oka *et al*. 2014, allele designation *Ywhae*$^{tm2.1Awb}$, genetic background 129S6/SvEvTac × C57BL/6J (9,14); for Wachi *et al*. 2017, allele designation *Ywhae*^{tm1Awb}, genetic background 129S6/SvEvTac (13); and for Ingham *et al*. and this study, allele designation *Ywhae*$^{tm1e(EUCOMM)Wtsi}$, genetic background C57BL/6N × 129S5/SvEvBrd/Wtsi (15).

Table 2. Full description of the *YWHAE* phenotypic and molecular findings in the study's cohort. Cases in blue have a variant limited to *YWHAE*. Cases with a yellow header have already been published. CMA: chromosomal microarray analysis. CT: computed tomography. EEG: electroencephalogram. GH: growth hormone. IUGR: intrauterine growth retardation. mo: months old. MRI: magnetic resonance imaging. NA: not available or not applicable. p.: percentile. SD: standard deviation. VSD: ventricular septal defect. VUR: vesicoureteral reflux. wg: weeks of gestation. yo: years old.

Figure 1. *YWHAE* variants reported in this study and analysis of splice site variant. (**A**) *YWHAE* variants at the gene level shown using the UCSC Genome Browser tool (39) (GRCh37 assembly): single nucleotide variants in cases 1, 2 and 3 and deletions <1 Mb encompassing *YWHAE* in cases 4 to 15. Five cases present with variants specifically in *YWHAE*, including 3 splice variants and 2 intragenic deletions. Genes highlighted in green are reported in OMIM to be disease-causing while genes in gray are not disease causing. *YWHAE* location is depicted in cyan. Coding exonic regions are depicted with gray shading. (**B**) Variants in cases 1, 2 and 3 are positioned at the protein level (NM_006761.5 NP_006752.1). Coding exon regions and 14-3-3 domain are depicted with gray shading. (**C**) Left panel: analysis by gel electrophoresis of exons 2 to 6 RT-PCR products from cases 2 and 3 showing two bands corresponding to two RNAs of different sizes. Right panel: study of variant impact on pre-messenger RNA splicing using targeted RNA deep sequencing showing heterozygous exon 5 skipping.

Figure 2. Brain MRIs and photographs in patients. (**A**) Brain MRI images of cases 1 (at 6 months old), 2 and 3 (at 3 years old). (**a-c**) T1 weighted sagittal brain MRI. (**a**) Case 1: pituitary hypoplasia (arrow). (**b**) Case 2: ventricular dilatation, enlarged Virchow-Robin spaces (arrowheads), germinolytic cysts (star) and thin corpus callosum. (**c**) Case 3: ventricular dilatation, enlarged Virchow-Robin spaces (arrowheads) and thin corpus callosum. (**d-j**) T1 weighted axial brain MRI. (**d**) Case 2: enlarged Virchow-Robin spaces (arrowheads). (**e**) Case 3: enlarged Virchow-Robin spaces (arrowheads). (**f**) Case 2: ventricular dilatation, germinolytic cysts (star). (**g**) Case 3: ventricular dilatation, septum pellucidum cyst (cross). (**h**) Case 3: ventricular dilatation, cavum vergae cyst (arrow). (**i**) Case 2: cerebellar vermis hypoplasia (arrow). (**j**) Case 3: cerebellar vermis hypoplasia (arrow). (**k**) T2 weighted coronal brain MRI in case 1: presence of the olfactory bulbs. (**l**) T2 FRFSE (Fast Recovery Fast Spin Echo) weighted coronal brain MRI in case 2: absence of the olfactory bulbs. (**m**) T2 FSE weighted coronal brain MRI in case 3: absence of the olfactory bulbs. (**n-o**) T2 FLAIR weighted axial

brain MRI. (**n**) Case 2: isointense white matter, with loss of gray/white dedifferentiation and hypersignal of the posterior white matter showing delayed myelination with age (arrow). (**o**) Case 3: isointense white matter, with loss of gray/white dedifferentiation showing delayed myelination with age, ventricular dilatation, septum pellucidum (cross) and cavum vergae cysts (arrow). (**B**) Photographs of cases 1, 4 and 10 from top to bottom.

Figure 3. *Ywhae*$^{tm1e/tm1e}$ mice display an array of developmental and neuroanatomical phenotypes. (**A**) Body weight in *Ywhae*$^{tm1e/tm1e}$ male mice from 4 to 16 weeks reproduced from Ingham et al. (15). (**B-C**) Body length and mean mass. (**D**) Cumulative food consumption over 21 hours measured in calorimetric cages. (**E**) Fat mass at 14 weeks. (**F-H**). Bone area, mineral content and density (14 weeks). (**I**) Histogram with fold increase/decrease expressed as percentage of wild-type mice. Plain lines regroup parameters or left and right hemispheres. Dotted lines indicate left and right hemispheres. Colored regions indicate the presence of at least one significant parameter within the brain region at the 0.05 level. TBA: total brain area. LV: lateral ventricles. Cg: cingulate cortex. gcc: genu of the corpus callosum. cc: corpus callosum. CPu: caudate putamen. aca: anterior commissure. Pir: piriform cortex. M1: primary motor cortex. S2: second somatosensory cortex. (**J**) Schematic representation of affected brain regions in mice plotted in coronal planes (Bregma +0.98mm) according to p-values. The color map indicates p-value below the threshold of 0.05 or grey where the n was too low to calculate statistics. (**K**) Nissl-stained coronal brain sections from WT and *Ywhae*$^{tm1e/tm1e}$ mice, showing the reduction of the cingulate cortex (Cg), the reduction of the width of the genu of the corpus callosum (gcc), the enlargement of the lateral ventricles (LV) and an unusual mass of axons beneath the genu of the corpus callosum at the midline (black arrow). (**L**) HREM analysis of 14.5 embryos showing on the left, enlarged ventricle (parasagittal sections) and on the right panel, the thinning of the cortical plate (CxP) and subventricular layer cortex (SubVCx) (coronal sections). The vertical blue lines on the parasagittal section (left) indicate the

corresponding coronal plane (shown on right panel) whilst the horizontal blue lines indicate the corresponding longitudinal plane (not shown) using ImageJ plugins.

Data availability

The datasets generated during this study are available upon request from the corresponding authors.

Acknowledgements

We thank the families for taking part in the study. We thank the CCuB for technical support and management of the computing platform. We thank ERN-ITHACA and the GeneMatcher platform for data sharing. Several authors are members of ERN-ITHACA. We acknowledge Christophe Ouzouf, Jérémie Roquet, Mathieu Chopelet and Laura Fenlon for discussion or providing comments on the manuscript. We thank the members of the Sanger Institute Mouse Pipelines teams and the Research Support Facility for the provision and management of the *Ywhae*$^{tm1e/tm1e}$ knockout mice.

Funding

This work was supported by grants from the French National Institute of Health and Medical Research (First Step to BY), the French National Research Agency (ANR JCJC to BY), the European Union through the FEDER program (to GAD) and by the Wellcome Trust Grant 206194. The Deciphering the Mechanisms of Developmental Disorders (DMDD) program was funded by the Wellcome Trust (Grant 100160) with support from the Francis Crick Institute, licensed under a Creative Commons Attribution license (CC BY V 4.0). The funders had no role in study design, data collection and analysis, decision to publish, or preparation of the manuscript.

Author contribution

Data curation: A.S.D.P.; V.E.; J.A.R.; C.J.L. Investigation: A.S.D.P.; S.C.C.; A.L.B.; A.M.; C.W.; V.E.V.; C.E.P.; M.P.B.; F.S.S.; M.P.M.; T.B.; E.L.; C.A.B.; J.A.R.; M.E.; M.A.M.; J.L.; B.D.; C.J.L.. Resources: V.E.V.; C.J.L. Software: Y.D. Supervision: A.S.D.P.; L.F.; B.Y. Writing-original draft: A.S.D.P.; S.C.C.; B.Y. Writing-review and editing: A.S.D.P.; A.L.B.; V.E.V.; Q.T.; C.E.P.; E.L.; J.A.R.; C.P.; L.F.; B.Y.

Ethics Declaration

This study conforms to the Helsinki Declaration of ethical principles for medical research involving human subjects. When additional analyses not included in the care approach were required (RNA studies), they were done in the framework of the DISCOVERY project which was approved by the appropriate French independent ethics committee (Comité de Protection des Personnes 2016-A01347-44), and samples were part of the GAD collection DC2011-1332. The care and use of mice were in accordance with the UK Home Office regulations, UK Animals (Scientific Procedures) Act of 1986. Permission was obtained to publish photographs of cases 1, 4 and 10.

Disclosure

We have no financial conflicts of interest to disclose.

References

1. Chong SS, Pack SD, Roschke AV, Tanigami A, Carrozzo R, Smith AC, et al. A revision of the lissencephaly and Miller-Dieker syndrome critical regions in chromosome 17p13.3. Hum Mol Genet. 1997 Feb;6(2):147–55.

2. Dobyns WB, Curry CJ, Hoyme HE, Turlington L, Ledbetter DH. Clinical and molecular diagnosis of Miller-Dieker syndrome. Am J Hum Genet. 1991 Mar;48(3):584–94.

3. Ledbetter SA, Kuwano A, Dobyns WB, Ledbetter DH. Microdeletions of chromosome 17p13 as a cause of isolated lissencephaly. Am J Hum Genet. 1992 Jan;50(1):182–9.

4. Jones KL, Gilbert EF, Kaveggia EG, Opitz JM. The MIller-Dieker syndrome. Pediatrics. 1980 Aug;66(2):277–81.

5. Cardoso C, Leventer RJ, Ward HL, Toyo-oka K, Chung J, Gross A, et al. Refinement of a 400-kb Critical Region Allows Genotypic Differentiation between Isolated Lissencephaly, Miller-Dieker Syndrome, and Other Phenotypes Secondary to Deletions of 17p13.3. Am J Hum Genet. 2003 Apr;72(4):918–30.

6. Noor A, Bogatan S, Watkins N, Meschino WS, Stavropoulos DJ. Disruption of YWHAE gene at 17p13.3 causes learning disabilities and brain abnormalities. Clin Genet. 2018 Feb;93(2):365–7.

7. Berg D, Holzmann C, Riess O. 14-3-3 proteins in the nervous system. Nat Rev Neurosci. 2003 Sep;4(9):752–62.

8. Li Q, Cheng Z, Zhou L, Darmanis S, Neff NF, Okamoto J, et al. Developmental Heterogeneity of Microglia and Brain Myeloid Cells Revealed by Deep Single-Cell RNA Sequencing. Neuron. 2019 Jan 16;101(2):207-223.e10.

9. Cornell B, Wachi T, Zhukarev V, Toyo-Oka K. Regulation of neuronal morphogenesis by 14-3-3epsilon (Ywhae) via the microtubule binding protein, doublecortin. Hum Mol Genet. 2016 Oct 15;25(20):4405–18.

10. Toyo-oka K, Shionoya A, Gambello MJ, Cardoso C, Leventer R, Ward HL, et al. 14-3-3epsilon is important for neuronal migration by binding to NUDEL: a molecular explanation for Miller-Dieker syndrome. Nat Genet. 2003 Jul;34(3):274–85.

11. Bi W, Sapir T, Shchelochkov OA, Zhang F, Withers MA, Hunter JV, et al. Increased LIS1 expression affects human and mouse brain development. Nat Genet. 2009 Feb;41(2):168–77.

12. Ikeda M, Hikita T, Taya S, Uraguchi-Asaki J, Toyo-oka K, Wynshaw-Boris A, et al. Identification of YWHAE, a gene encoding 14-3-3epsilon, as a possible susceptibility gene for schizophrenia. Hum Mol Genet. 2008 Oct 15;17(20):3212–22.

13. Wachi T, Cornell B, Toyo-Oka K. Complete ablation of the 14-3-3epsilon protein results in multiple defects in neuropsychiatric behaviors. Behav Brain Res. 2017 Feb 15;319:31–6.

14. Toyo-oka K, Wachi T, Hunt RF, Baraban SC, Taya S, Ramshaw H, et al. 14-3-3ε and ζ regulate neurogenesis and differentiation of neuronal progenitor cells in the developing brain. J Neurosci Off J Soc Neurosci. 2014 Sep 3;34(36):12168–81.

15. Ingham NJ, Pearson SA, Vancollie VE, Rook V, Lewis MA, Chen J, et al. Mouse screen reveals multiple new genes underlying mouse and human hearing loss. Freeman TC, editor. PLOS Biol. 2019 Apr 11;17(4):e3000194.

16. Sobreira N, Schiettecatte F, Valle D, Hamosh A. GeneMatcher: a matching tool for connecting investigators with an interest in the same gene. Hum Mutat. 2015 Oct;36(10):928–30.

17. Richards S, Aziz N, Bale S, Bick D, Das S, Gastier-Foster J, et al. Standards and guidelines for the interpretation of sequence variants: a joint consensus recommendation of the American College of Medical Genetics and Genomics and the Association for Molecular Pathology. Genet Med. 2015 May;17(5):405–23.

18. Skarnes WC, Rosen B, West AP, Koutsourakis M, Bushell W, Iyer V, et al. A conditional knockout resource for the genome-wide study of mouse gene function. Nature. 2011 Jun 15;474(7351):337–42.

19. Ryder E, Gleeson D, Sethi D, Vyas S, Miklejewska E, Dalvi P, et al. Molecular characterization of mutant mouse strains generated from the EUCOMM/KOMP-CSD ES cell resource. Mamm Genome Off J Int Mamm Genome Soc. 2013 Aug;24(7–8):286–94.

20. White JK, Gerdin AK, Karp NA, Ryder E, Buljan M, Bussell JN, et al. Genome-wide generation and systematic phenotyping of knockout mice reveals new roles for many genes. Cell. 2013 Jul 18;154(2):452–64.

21. Paxinos G, Franklin KBJ. The Mouse Brain in Stereotaxic Coordinates. 4th edition. Amsterdam: Academic Press; 2012. 360 p.

22. Mikhaleva A, Kannan M, Wagner C, Yalcin B. Histomorphological Phenotyping of the Adult Mouse Brain. Curr Protoc Mouse Biol. 2016 Sep 1;6(3):307–32.

23. Collins SC, Mikhaleva A, Vrcelj K, Vancollie VE, Wagner C, Demeure N, et al. Large-scale neuroanatomical study uncovers 198 gene associations in mouse brain morphogenesis. Nat Commun. 2019 Aug 1;10(1):3465.

24. Weninger WJ, Geyer SH, Mohun TJ, Rasskin-Gutman D, Matsui T, Ribeiro I, et al. High-resolution episcopic microscopy: a rapid technique for high detailed 3D analysis of gene activity in the context of tissue architecture and morphology. Anat Embryol (Berl). 2006 Jun;211(3):213–21.

25. Collins SC, Wagner C, Gagliardi L, Kretz PF, Fischer MC, Kessler P, et al. A Method for Parasagittal Sectioning for Neuroanatomical Quantification of Brain Structures in the Adult Mouse. Curr Protoc Mouse Biol. 2018 Sep;8(3):e48.

26. Romano C, Ferranti S, Mencarelli MA, Longo I, Renieri A, Grosso S. 17p13.3 microdeletion including YWHAE and CRK genes: towards a clinical characterization. Neurol Sci Off J Ital Neurol Soc Ital Soc Clin Neurophysiol. 2020 Aug;41(8):2259–62.

27. Mignon-Ravix C, Cacciagli P, El-Waly B, Moncla A, Milh M, Girard N, et al. Deletion of YWHAE in a patient with periventricular heterotopias and pronounced corpus callosum hypoplasia. J Med Genet. 2010 Feb 1;47(2):132–6.

28. Chen CP, Ko TM, Wang LK, Chern SR, Wu PS, Chen SW, et al. Prenatal diagnosis of a 0.7-Mb 17p13.3 microdeletion encompassing YWHAE and CRK but not PAFAH1B1 in a fetus without ultrasound abnormalities. Taiwan J Obstet Gynecol. 2018 Feb;57(1):128–32.

29. Schiff M, Delahaye A, Andrieux J, Sanlaville D, Vincent-Delorme C, Aboura A, et al. Further delineation of the 17p13.3 microdeletion involving YWHAE but distal to PAFAH1B1: Four additional patients. Eur J Med Genet. 2010 Sep;53(5):303–8.

30. Nagamani SCS, Zhang F, Shchelochkov OA, Bi W, Ou Z, Scaglia F, et al. Microdeletions including YWHAE in the Miller-Dieker syndrome region on chromosome 17p13.3 result in facial dysmorphisms, growth restriction, and cognitive impairment. J Med Genet. 2009 Dec;46(12):825–33.

31. Bruno DL, Anderlid BM, Lindstrand A, Ravenswaaij-Arts C van, Ganesamoorthy D, Lundin J, et al. Further molecular and clinical delineation of co-locating 17p13.3 microdeletions and microduplications that show distinctive phenotypes. J Med Genet. 2010 May 1;47(5):299–311.

32. Mire E, Hocine M, Bazellières E, Jungas T, Davy A, Chauvet S, et al. Developmental Upregulation of Ephrin-B1 Silences Sema3C/Neuropilin-1 Signaling during Post-crossing Navigation of Corpus Callosum Axons. Curr Biol CB. 2018 Jun 4;28(11):1768-1782.e4.

33. Paxinos G, Halliday GM, Watson C, Koutcherov Y, Wang H. Atlas of the Developing Mouse Brain at E17.5, P0 and P6. Academic Press; 2007. 378 p.

34. Karczewski KJ, Francioli LC, Tiao G, Cummings BB, Alföldi J, Wang Q, et al. The mutational constraint spectrum quantified from variation in 141,456 humans. Nature. 2020 May;581(7809):434–43.

35. Paul LK, Corsello C, Kennedy DP, Adolphs R. Agenesis of the corpus callosum and autism: a comprehensive comparison. Brain J Neurol. 2014 Jun;137(Pt 6):1813–29.

36. Yam PT, Kent CB, Morin S, Farmer WT, Alchini R, Lepelletier L, et al. 14-3-3 proteins regulate a cell-intrinsic switch from sonic hedgehog-mediated commissural axon attraction to repulsion after midline crossing. Neuron. 2012 Nov 21;76(4):735–49.

37. Yang T, Terman JR. 14-3-3ε couples protein kinase A to semaphorin signaling and silences plexin RasGAP-mediated axonal repulsion. Neuron. 2012 Apr 12;74(1):108–21.

38. Moon HM, Wynshaw-Boris A. Cytoskeleton in action: lissencephaly, a neuronal migration disorder. Wiley Interdiscip Rev Dev Biol. 2013 Apr;2(2):229–45.

39. Kent WJ, Sugnet CW, Furey TS, Roskin KM, Pringle TH, Zahler AM, et al. The Human Genome Browser at UCSC. Genome Res. 2002 Jan 6;12(6):996–1006.

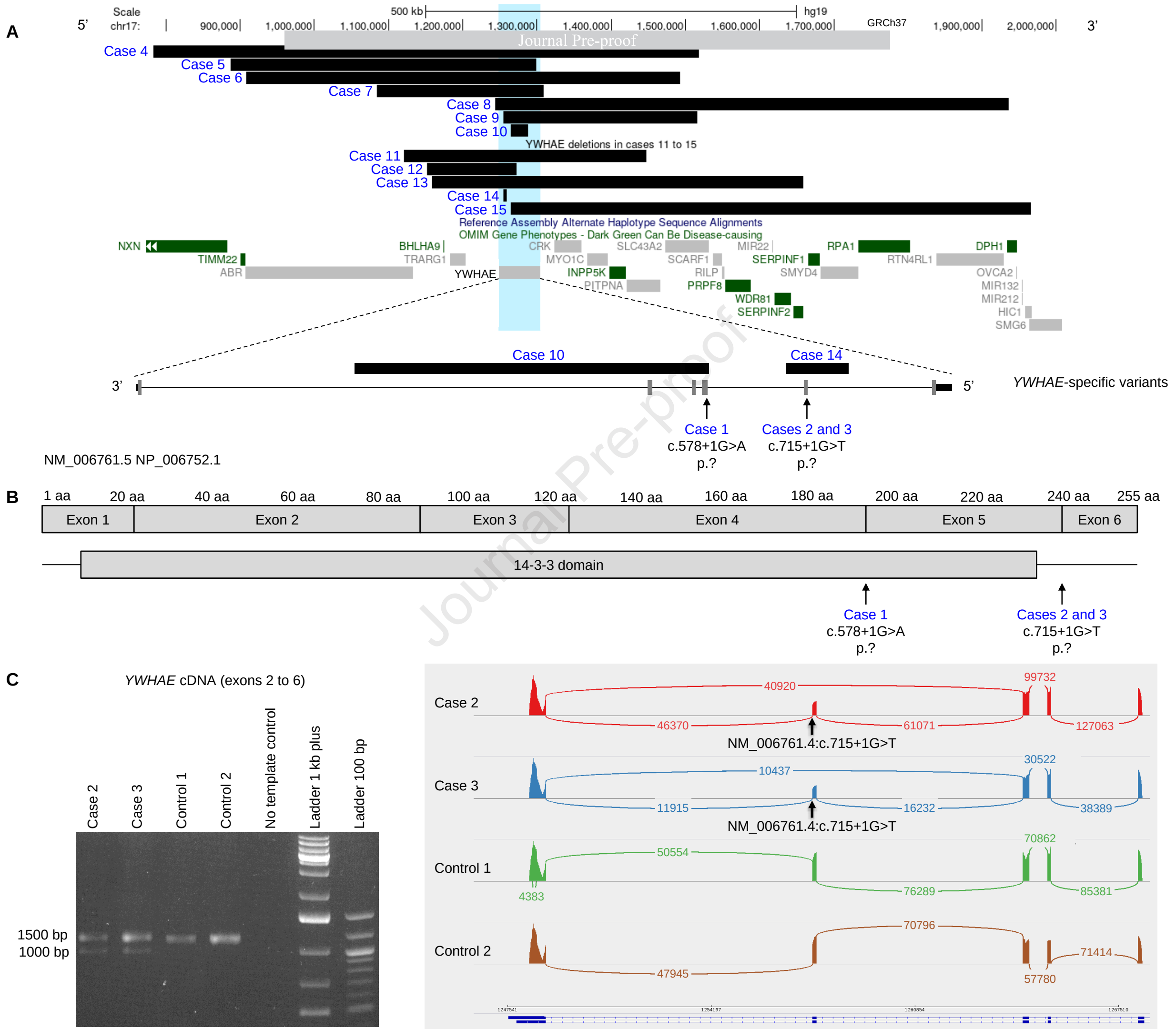

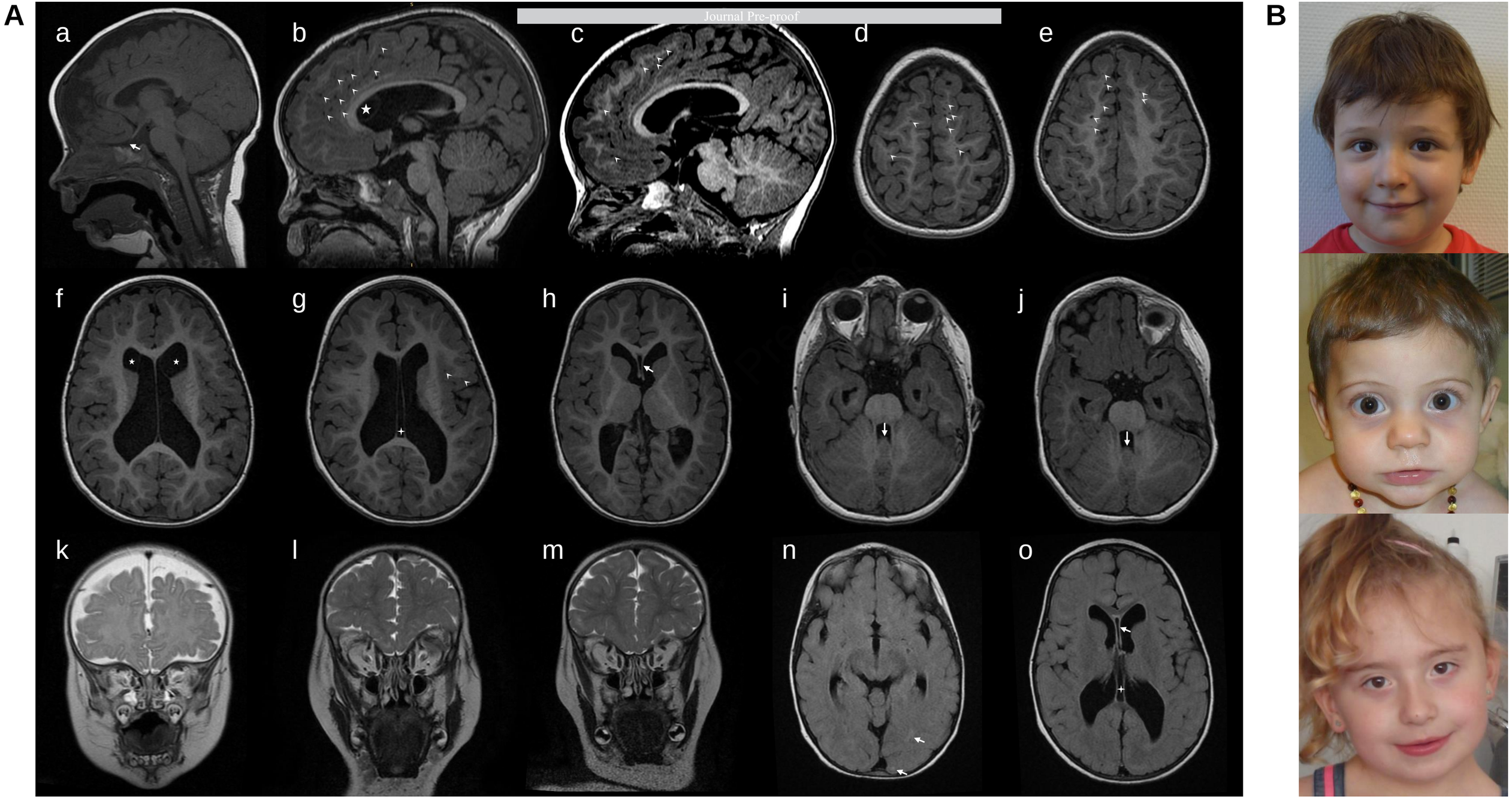

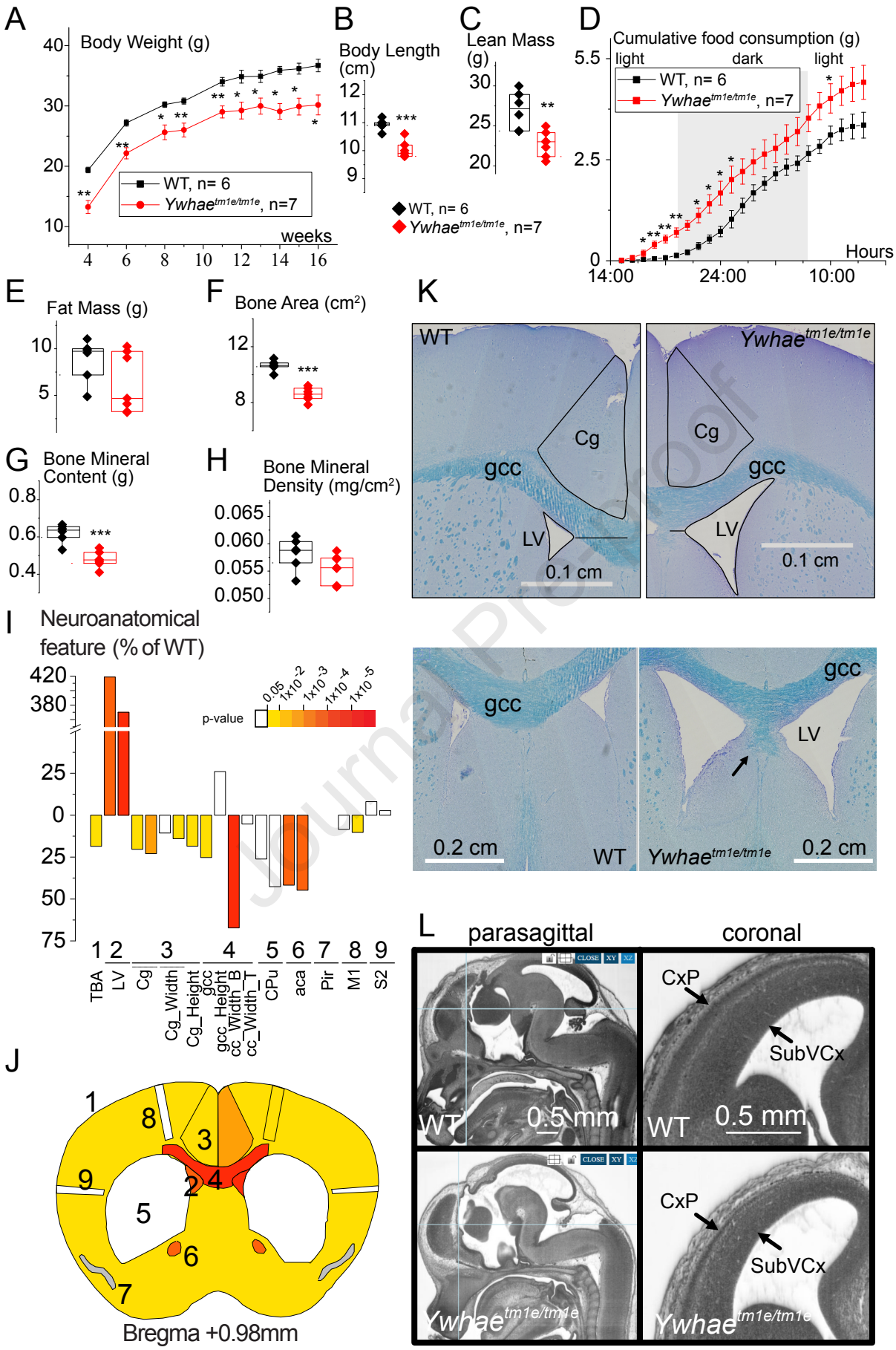

Clinical features	Variants in *YWHAE* only	Variants in *YWHAE* and other genes	Total	*Ywhae*$^{+/-}$ mice Literature	*Ywhae*$^{-/-}$ mice Literature	*Ywhae*$^{-/-}$ mice This study
Developmental delay	5/5	8/9	13/14	Not available	+ (Wachi 2017)	Not available
Intellectual disability	1/5 (mild)	5/8 (mild to severe)	6/13	Not available	Not available	Not available
- Memory impairment	Not available	Not available	Not available	+ (Ikeda 2008)	+ (Wachi 2017)	Not available
Delayed or impaired speech	5/5	6/6	11/11	Not available	Not available	Not available
Hypotonia	4/4	3/8	7/12	+ (Wachi 2017)	++ (Wachi 2017)	Not available
Seizures	4/5	4/8	8/13	Not available	Not available	Not available
Behavioral disorder	3/4	3/8	6/12	+ Hyperactivity (Ikeda 2008, Wachi 2017)	++ (Wachi 2017)	+
Anxiety	2/4	1/8	3/12	+/- (Ikeda 2008, Wachi 2017)	Not available	Not available
Brain malformations	4/4	4/8	8/12	+ (Toyo-Aka 2003)	++ (Toyo-Aka 2003)	+
- Corpus callosum hypoplasia	3/4	2/7	5/11	Not available	Not available	++
- Ventricular dilatation	2/4	1/7	3/11	Not available	Not available	+++
- Poor myelination	2/4	1/7	3/11	Not available	Not available	Not available
- Cortical hypoplasia	0/4	2/7	2/11	+ (Toyo-Aka 2003)	++ (Toyo-Aka 2003)	++
- Hippocampal defects	Not reported	Not reported	Not reported	+ (Toyo-Aka 2003)	++ (Toyo-Aka 2003)	Not available

Growth retardation	0/4	4/7	4/11	+/- (Ikeda 2008, Wachi 2017)	++ (Toyo-Aka 2003, Wachi 2017, Ingham 2019)	+
Craniofacial features	3/5	9/10	12/15	Not available	+ (shortened skull, Ingham 2019)	+ (shortened skull)
Hearing impairment	Not reported	Not reported	Not reported	Not available	Moderate (Ingham 2019)	Not available

Cases	1	2	3	4	5	6	7	8	9	10	11	12	13	14	15
Publication	This study	This study	This study	PMID 32323081 (Romano *et al.*) Follow-up	PMID 19635726 (Mignon-Ravix *et al.*) Follow-up	This study	This study	This study	This study	This study	PMID 20452996 (Bruno *et al.*, patient 3)	PMID 19584063 (Sreenath Nagamani *et al.*, patient 1)	PMID 20599530 (Schiff *et al.*, patient D)	PMID 28542865 (Noor *et al.*)	PMID 29458882 (Chen *et al.*)
Variant	NM_006761.5:c.578+1G>A p.?	NM_006761.5:c.715+1G>T p.(Leu194*)	NM_006761.5:c.715+1G>T p.(Leu194*)	arr[GRCh37] 17p13.3(783542_1518383)x1	arr[GRCh37] 17p13.3(887704_1298810)x1	arr[GRCh37] 17p13.3(908480_1492475)x1.ish del(17)(p13.3p13.3) (RP11-818024-)dn	arr[GRCh37] 17p13.3(1084016_1308796)x1dn	arr[GRCh37] 17p13.3 (1244153_1935766)x1	arr[GRCh37] 17p13.3(1254875_1516480)x1dn	arr[GRCh37] 17p13.3(1264229_1288574)x1	arr[GRCh37] 17p13.3(1120324_1447883)x1dn	arr[GRCh37] 17p13.3(1151382_1272389)x1dn	arr[GRCh37] 17p13.3 (1158449_1658551)x1	arr[GRCh37] 17p13.3 (1254694_1258917)x1dn	arr[GRCh37] 17p13.3(1264243_1965733)x1dn
Deletion (included genes)	NA (*YWHAE*)	NA (*YWHAE*)	NA (*YWHAE*)	735kb (*MRM3, NXN, TIMM22, ABR, BHLHA9, TRARG1, YWHAE, CRK, MYO1C, INPP5K, PITPNA-AS1, PITPNA*)	411kb (*TIMM22, ABR, BHLHA9, TRARG1, YWHAE*)	584kb (*ABR, BHLH9, TRARG1, YWHAE, CRK, MYO5C, INPP5K, PITPNA-AS1, PITPNA, SLC43A2*)	224kb (*ABR, BHLHA9, TRARG1, YWHAE*)	692kb (*YWHAE, CRK, MYO1C, INPP5K, PITPNA-AS1, PITPNA, SLC43A2, SCARF1, RILP, PRPF8, TLCD2, WDR81, SERPINF2, SMYD4, RPA1, RTN4RL1, OPH1*)	262kb (*YWHAE, CRK, MYO1C, INPP5K, PITPNA-AS1, PITPNA, SLC43A2, RN7SL105P*)	24kb (*YWHAE*, exons 2 to 4)	328kb (*ABR, BHLHA9, CRK, INPP5K, MYO1C, PITPNA, PITPNA-AS1, TRARG1, YWHAE*)	121kb (*BHLHA9, TRARG1, YWHAE*)	500kb (*BHLHA9, TRARG1, YWHAE, CRK, MYO1C, INPP5K, PITPNA-AS1, PITPNA, SLC43A2, RN7SL105P, SCARF1, RILP, PRPF8, TLCD2, MIR22HG, MIR22, WDR81, SERPINF2*)	12.6kb (*YWHAE*, exon 5)	701kb (*YWHAE, CRK, MYO1C, INPP5K, PITPNA-AS1, PITPNA, SLC43A2, SCARF1, RILP, PRPF8, TLCD2, WDR81, SERPINF2, SMYD4, RPA1*)
Inheritance	*De novo*	*De novo*	*De novo*	Inherited from healthy father (paternal mosaicism)	NA (father not available)	*De novo*	*De novo*	NA	*De novo*	Inherited from affected father (minor phenotype)	*De novo*	*De novo*	NA	*De novo*	*De novo*
Classification	Pathogenic (PVS1, PS2, PM2)	Pathogenic (PVS1, PS2, PM2)	Pathogenic (PVS1, PS2, PM2)	Pathogenic	Pathogenic	Pathogenic	Pathogenic	Pathogenic	Pathogenic	Pathogenic	Pathogenic	Pathogenic	Pathogenic	Pathogenic	Pathogenic
Technology of variant detection	Multigene panel (1637 genes)	Exome sequencing	Exome sequencing	CMA	CMA	CMA	CMA	CMA	CMA	CMA	CMA	CMA	CMA	CMA	CMA
Sex	Male	Female	Female	Female	Male	Female	Female	Female	Male	Female	Male	Male	Male	Male	NA
Gestational age	38+2 wg	30 wg	30 wg	39+2 wg	41+5 wg	38 wg	41+6 wg	NA	39 + 5 wg	38 wg	36+4 wg	NA	37 wg	At term	19 wg
Length at birth	49 cm (50th p.)	41.5 cm (90th p.)	41 cm (50-90th p.)	46 cm (3-10th p.)	49.5 cm (10th p.)	NA	51 cm (10-50th p.)	NA	48 cm (10th p.)	47.5 cm (10-50th p.)	46 cm (10-50th p.)	NA	44 cm (3rd p.)	NA	NA
Weight at birth	2820 g (10-50th p.)	1520 g (50-90th p.)	1695 g (90th p.)	2550 g (3-10th p.)	3260 g (10th p.)	2752 g (10-50th p.)	3340 g (10-50th p.)	NA	2878 g (10th p.)	3025 g (50th p.)	2270 (10th p.)	3180 g	2400 g (10th p.)	3700 g (50-90th p.)	268 g
Head circumference at birth	33.5 cm (50th p.)	30 cm (97th p.)	30 cm (97th p.)	33 cm (10th p.)	38 cm (95th p.)	NA	NA	NA	35 cm (50th p.)	32.5 cm (10-50th p.)	Normal	NA	33.5 cm (50th p.)	NA	NA
Prenatal features	Normal	Normal	Normal	IUGR, oligohydramnios	Normal	Polyhydramnios	Normal	Normal	SARS-CoV-2 infection (1st trimester)	Nuchal translucency	NA	No	NA	NA	NA
Age at last evaluation	3 yo 10 mo	10 yo 4 mo	10 yo 4 mo	4 yo	13 yo	14 yo	14 yo	39 yo	11.5 mo	5 yo 3 mo	NA	13 yo	4 yo	8 yo 4 mo	19 wg
Weight	17.5 kg (+0.5 SD)	24 kg (-2 SD)	24 kg (-2 SD)	NA	36 kg (-1 SD)	25.9 kg (-3 SD)	NA	NA	10.33 kg (+0.5 SD)	26 kg (+2 SD)	NA	47 kg (M)	12.6 kg (-2.3 SD)	NA	268 g
Height	101 cm (M)	128 cm (-1.7 SD)	128 cm (-1.7 SD)	NA	132 cm (-2.5 SD)	124.3 cm (-5.5 SD)	NA	NA	77 cm (+1 SD)	115 cm (+1 SD)	NA	145.4 cm (-1.3 SD)	93 cm (-2.5 SD)	NA	NA
Head circumference	53 cm (+1.6 SD)	52.7 cm at 8 yo 10 mo (+0.5 SD)	52 cm at 8 yo 10 mo (M)	NA	58.5 cm (+3 SD)	51.6 cm (-2 SD)	NA	57.3 cm (+1.5 SD)	48 cm (+1 SD)	52 cm (+1 SD)	NA	49.7 cm (-3 SD)	51.5 cm (+0.5 SD)	NA	NA

Growth retardation	No	No	No	NA	Yes	Yes	NA	No	No	No	Yes	No	Yes	NA	NA
DD	Yes	Yes	Yes	Yes	Yes	Yes	Yes	Yes	No	Yes	Yes	Yes	Mild to moderate	Yes	NA
ID	Mild	No	No	Mild	Mild to moderate	No	Moderate to severe	Mild	NA	No	No	Mild to moderate	No	No	NA
Walking age	18 mo	30 mo	30 mo	18 mo	30 mo	12-13 mo	< 12 mo	NA	NA	16.5 mo	NA	NA	12 mo	Normal	NA
Gait	Impaired	Normal	Normal	NA	Impaired	Normal	Impaired	Normal	NA	NA	NA	NA	Normal	NA	NA
Hand skills	Impaired (difficulties in fine motor)	Dyspraxia	Dyspraxia	NA	Normal	Normal	NA	NA	Normal	Impaired	NA	NA	NA	NA	NA
Age at first sentence	2.5 yo	2.5 yo	2.5 yo	NA	NA	2-3 yo	> 3 yo	NA	NA	NA	NA	NA	First word at 40 mo	NA	NA
Speech/language development or troubles	Make sentence, difficulties in articulation	Dysphasia	Dysphasia	Impaired	Impaired, reading acquired	Impaired, some words at 13 yo	Impaired	Impaired, poor articulation, nasal voice	NA	Impaired	NA	NA	Delayed	Dysgraphia	NA
Seizures	Generalized febrile seizure	Tonicoclonic, multi-daily absences	No	Daily seizures, brisk episodes of head, limbs flexion on trunk, awakening and crying	No	No	Tonicoclonic, myoclonic and absence seizures	Only one epileptic seizure	Infantile spasms	Eye revulsions	NA	No	No	Myoclonic	NA
Age at first seizure	16 mo (only one seizure)	9 yo	NA	5 mo	NA	NA	1 yo	NA	4.5 mo	NA	NA	NA	NA	2.5 yo	NA
Seizure treatment	No	Levetiracetam (no effective) and valproate (effective)	NA	Vigabatrin followed by one ACTH cycle	NA	NA	Drug resistant, anticonvulsants and spinal cord stimulator	No	Vigabatrin, prednisolone and ketogenic diet	NA	NA	NA	NA	Ethosuximide	NA
EEG	Normal	Discontinuous pattern, abundant theta frequencies, bilateral temporal positive spikes	NA	Strong diffuse multifocal paroxysmal activity (spike-and-wake and polyspike-and-wave)	NA	NA	Disorganized sleep and wake patterns, rather diffuse abnormalities during sleep	Irregular spike-wave complexes on the right side	Infantile spasms, wake and sleep differentiated at the diagnosis of infantile spasms and at the last follow up the EEG was normal	NA	NA	NA	NA	NA	NA
Brain MRI or CT	Pituitary hypoplasia, small unilateral arachnoid cyst	Intraventricular hemorrhage, germinolytic cyst, ventricular dilatation, absence of the olfactory bulbs, hypoplasia of the cerebral white matter, thin corpus callosum, enlarged Virchow-Robin spaces, cerebellar vermis hypoplasia	Ventricular dilatation, cyst of the septum pellucidum and the cavum vergae, thin corpus callosum and enlarged Virchow-Robin spaces, delayed myelination, cerebellar vermis hypoplasia, absence of the olfactory bulbs	Slight widening of anterior portion of left sylvian fissure, reduced volume of inferior frontal parenchyma with widening of ipsilateral superficial liquor spaces, poor myelination	Nodular heterotopias, hypoplasia of the corpus callosum, polymicrogyria, abnormal bulging of the brainstem	Normal	Normal	NA	Normal (thalamic restriction: vigabatrin?)	NA	Not performed	Thinning of corpus callosum and frontal cortex	Colobomatous cyst near right optic nerve, normal aspect of the white matter and enlarged Virchow-Robin spaces	Chiari I, thin corpus callosum, thin cavum septum pellucidum and cavum vergae	NA

Behavioral disorders	No	Anxiety, skin scratching, ADHD, short attention span	Anxiety, skin scratching, ADHD, short attention span	NA	Yes	No	Low frustration tolerance	Anxiety, obsessive compulsive behavior, self injury, always looking food, abnormal temper tantrums, skin scratching	No	ADHD	No	No	No	NA	NA
Neuromuscular abnormalities	Hypotonia	Hypotonia in early childhood	Hypotonia in early childhood	NA	Normal	Occasional tremors	Normal	Intentional tremors	Hypotonia	Hypotonia	Hypotonia	Mild hypotonia	No	NA	NA
Eye abnormalities	Nystagmus, strabismus, mild hypoplasia of optic nerve	No	No	No	Strabismus, nystagmus, hypertelorism	Mild hypertelorism	No	No	No	No	Iris coloboma	No	Hypertelorism, right microcornea, ptosis, bilateral chorioretinal and lens coloboma	No	NA
Epicanthus	No	No	No	No	Yes	Yes	No	No	No	Yes	No	Yes	No	No	Yes
Downslanting palpebral fissures	No	No	No	No	Yes	No	No	No	No	Yes	Yes	Yes	Yes	No	No
Ear abnormalities	No	No	No	Folded left ear helix	Small, low set and posteriorly rotated, thick and irregular helix	No	No	No	No	No	Low set ears, cupped	Low set ears, large auricles	No	Low set ears	Low set ears
Other craniofacial features	Sparse eyebrows	No	No	Slight periorbital edema, thin upper and thick lower lip, arched eyebrows, flat nasal root, bulbous nasal tip	Prominent forehead, pronounced cupid bow, macrocephaly, anteverted nares	NA	Dark circles around the eyes	Large head	No	Thin upper lip	Broad face, normal forehead, laterally extended eyebrows, broad nasal tip and base, micrognathia, thick and everted upper lip	Prominent forehead, tall vertex, retrognathia, thin upper lip	Large face, short nose, everted lower lip, pointed chin	Prominent forehead and occiput, bitemporal narrowing, furrowed brow, broad nasal root, anteverted nostrils, micrognathia	Microcephaly, broad nasal bridge, anteverted nostrils, micrognathia
Skeletal defects	Hyperlaxity	Clinodactyly of the 4th and 5th fingers	Clinodactyly of the 5th fingers	Clinodactyly of the 5th fingers	No	No	Camptodactyly of the 5th fingers, familial syndactyly of 2nd and 3rd toes	Genu recurvatum, large hands and feet	No	No	No	Arthrogryposis of upper limbs	No	NA	NA
Gastrointestinal features	No	Abdominal pain, tympanites, diarrhea, cow's milk protein intolerance	Abdominal pain, tympanites, diarrhea, cow's milk protein intolerance	No	No	Feeding difficulties in early infancy, swallow studies showed laryngeal penetration	No	No	Constipation	No	Neonatal feeding difficulties	No	No	NA	NA
Urogenital and kidney abnormalities	No	Enuresis nocturna	No	No	Unilateral cryptorchidism	No	No	No	No	No	NA	Anteriorly placed anus, VUR, hydronephrosis	No	NA	NA
Cardiac anomalies	No	No	Valvular pulmonary stenosis, VSD spontaneously resolved	No	No	No	No	No	Ventricular extrasystoles	NA	NA	NA	No	NA	NA

Skin abnormalities	No	Congenital nevus	No	No	No	No	Five small cafe-au-lait spots	Scratching and skin papules	No	No	NA	No	No	NA	NA
Endocrine dysfunction	No	No	No	No	Thyrotropic and corticotropic deficit substituted since age 13	GH deficiency treated by GH supplementation since age 9	NA	Diabetes mellitus, high triglycerides, GH deficiency treated by GH during childhood	No	NA	NA	NA	No	NA	NA
Other		Anosmia, enamel brittleness	Anosmia, abnormal enamel					Neonatal hyperbilirubinemia with exchange transfusion, fat accumulation hips, daytime sleepiness, low neutrophils	No		No recurrent infections	No	No	Learning difficulties related to mathematics	